

# 4 Systematic search for systems with S-shaped current–potential characteristics

## 4.1 Introduction

As mentioned in chapter 1, a recent theoretical study predicts that Turing patterns emerge easily in electrochemical systems with an S-shaped current–double layer potential characteristic [28]. In these systems, the double layer potential acts as the inhibitor, and a chemical quantity, such as the concentration of an electroactive species or the coverage of the electrode by an adsorbate, acts as the activator. Spatial inhomogeneities in the double layer potential and the concentration or the adsorbate coverage induce diffusion and migration fluxes, respectively, and the typical time scale associated with migration is much shorter than that associated with diffusion. Hence, the transport process linked to the inhibitor is faster than the one linked to the activator. That the transport process of the inhibitor is faster than the one of the activator is just the critical requirement an activator–inhibitor system has to meet in order to form Turing structures. Because the requirement is met by any electrochemical system with an S-shaped current–potential characteristic, the prediction is not only exciting from the point of view of the nonlinear dynamics, and this especially in view of the very few experimental examples of Turing structures, but also of importance in the electrochemical context.

A successful study of the predicted Turing patterns requires an electrochemical system with the following properties: (a) It should possess an S-shaped current–potential characteristic. (b) The mechanism, generating the ‘S’, should be known in order (i) to exclude further nonlinear steps which interfere with the dynamics and (ii) to be able to control the system with external parameters (e.g., concentration of electroactive species) in an optimal way. (c) The two branches of the ‘S’ should possess a sufficient contrast in SPI, which requires that the reaction proceeds on a Au electrode. Since a system fulfilling all these requirements was

not described in literature, we stepwise designed it. This design of a suitable system with S-shaped current-potential characteristic is described in this chapter.

An S-shaped current-potential curve is characterized by a potential region, in which three stationary current densities exist for a given value of the electrode potential. Two of these values are locally stable and can be realized in an experiment, whereas one, more precisely the one that corresponds to the middle branch of the 'S', is unstable. Hence, the system is bistable. This is the simplest non-equilibrium phenomenon. A related situation exists in equilibrium systems, which undergo a first-order phase transition. Here, a globally stable and a metastable state coexist, and they are separated by a completely unstable state. As far as electrochemical systems are concerned, many organic adsorbates are known to undergo a first-order phase transition as a function of the electrode potential. In these systems the electrode is in contact with an electrolyte, in which the organic compound is dissolved. In certain potential regions the tendency of the organic species to adsorb at the electrode is very low, such that the equilibrium coverage is minimal. Hence, the adsorbate can be considered to form a two-dimensional gas. Upon variation of the potential - in most cases toward the point of zero charge - the coverage starts to increase. If the adsorbate molecules exert attractive interactions among each other, there is a sudden increase in coverage, often towards a completely ordered monolayer, once the coverage exceeds a certain threshold. This sudden increase in coverage is due to a first-order phase transition, whereby the two phases are characterized by a two-dimensional gas-like state, and a two-dimensional solid.

In principle, it should be possible to transform such a phase transition system into a bistable system with an S-shaped current-potential curve by superimposing an electrochemical reaction, which is inhibited by the condensed, well ordered adsorbate layer but proceeds in a nearly unhindered way in parameter regions, in which the gas-like state exists. Consider, for example, an adsorbate that forms a condensed phase around the point of zero charge and undergoes the above described phase transition at some more negative potential. Furthermore, consider a reduction reaction, i.e., a reaction, whose driving force increases towards negative potentials, and assume that the reaction is inhibited

by the condensed state. Then the current will be close to zero, as long as the condensed state exists, and will increase jump-like at the potential, at which the phase transition occurs. Upon decreasing the potential, a similar jump towards the low current density state occurs. For any finite scan rate, the potential at which this jump occurs, is more negative for the scan towards negative potential values than on the reverse scan towards positive values. This hysteresis occurs because of the activation energy, which has to be overcome to form the critical nuclei which initiate the phase transition. Obviously, the resulting current-potential curve is bistable, and supplementing the curve by the unstable state, the stationary states trace out an S-shaped curve. Thus, the combination of a first-order phase transition of an organic molecule and a redox reaction should lead to an S-shaped current-potential curve. Such systems also possess the other above mentioned properties, namely first, the mechanism, which generates the S-shaped current-potential curve, is well understood, and second, since organic adsorbates cause a considerable change in the optical properties of the electrode/electrolyte interface, it is likely that there will be a sufficient contrast for SPR imaging. Hence, our construction of an electrochemical system with an S-shaped current-potential curve consisted of two steps: 1) to find a suitable organic adsorbate and 2) a suitable redox reaction. From literature it is known that, among others, thymine, coumarin, and camphor can adsorb on gold single crystal electrodes and form a condensed film through a first-order phase transition [56-61]. These three molecules were selected as 'test molecules' in our studies from those which are known to exhibit a first-order phase transition because they are among those that were most intensively investigated. Furthermore, they are chemically different, so that it is also expected that the contrast in SPR will be different and the nature of the attractive interactions is different. Hydrogen bridges, e.g., are responsible for the formation of the condensed thymine film, whereas Van der Waals forces cause the phase transition in the case of camphor. Hence, the systems might be differently sensitive towards imperfections of the electrode surface. This is an important aspect because it is known that no phase transition (PT) occurs on polycrystalline electrodes. Au film electrodes, which are used in the present study, can be prepared such that the surface is predominantly made of (111) terraces. However, it is always less perfect than the surface of a bulk single crystal.

As for the redox species, the search turned out to be more difficult. The strategy we followed was first to test those with a most simple charge transfer mechanism, which proceeds directly from a complexed cation to the electrode without any chemical interactions involved. Two classical outer sphere redox systems are  $[\text{Ru}(\text{NH}_3)_6]^{3+}/[\text{Ru}(\text{NH}_3)_6]^{2+}$  and  $\text{Fe}(\text{CN})_6^{3-}/\text{Fe}(\text{CN})_6^{4-}$ . Since both systems did not yield the desired behavior, we turned to persulfate reduction, which was reported to be strongly inhibited by a camphor adlayer on Hg [62, 63] as well as by a chimolin adlayer on Hg [64], to hydrogen peroxide reduction, where a peroxy-bond is broken, and to periodate reduction, which was also reported to be inhibited by a condensed camphor film on Hg [65]. As will be demonstrated in section 4.3, essentially every redox system exhibited a different interaction with the organic condensed phase, just one of them possessing the desired properties.

The following two sections describe the electrochemical and SPR behavior of the three selected organic molecules at Au(111) film electrodes and the variety of different interactions between the organic condensed phases and the mentioned redox systems.

## **4.2 Search for an organic molecule with a good phase transition on the Au(111) film electrode**

As already mentioned, we investigated three organic molecules which had been studied before with single crystal Au(111) or mercury electrodes. Emphasis is on their phase transition behavior on our Au(111) film electrode. The decision of a good phase transition, which leads to the selection of the organic molecule in the studies on pattern formation, is based on two aspects: 1) The phase transition manifests itself in spike-like current peaks in the CV; the sharpness of these peaks was employed as an indication of the ability of the molecule to undergo a phase transition on the not ideal Au film electrodes and served at the same time as an indication of the quality of our surface. 2) Because we employ SP imaging in the pattern formation studies, the two phases should exhibit a contrast in the SPR signal.

## 4.2.1 Thymine

Thymine is a pyrimidine base with the chemical composition  $C_5H_6N_2O_2$  that is one of the four bases coding genetic information in the polynucleotide chain of DNA. The structure of its two tautomeric forms are shown in Fig. 4.1.

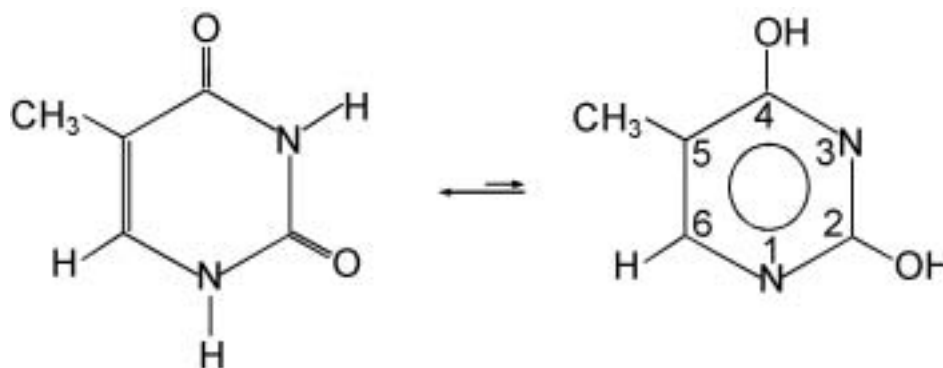


**Figure 4.1:** Tautomeric forms of a thymine molecule.

Thymine adsorption on electrode surfaces has been intensively studied on mercury as well as on well defined solid electrodes [57-59, 66]. The capacitance measurements as well as cyclic voltammetric investigations show that thymine exhibits three different adsorption states on the Au(111) electrode [57, 66]. As can be seen in the cyclic voltammogram reproduced from ref. [66] (Fig. 4.2 ), four potential regions can be distinguished [[57, 66] . In region I (-0.5 to -0.33 V vs. SCE, i.e., -0.91 to -0.74 vs. SMSE (-0.41 V) used in our experiments), thymine molecules randomly adsorb on the surface and form an ordered physisorbed phase at -0.33 V vs. SCE. This disorder-order phase transition is marked by a narrow peak at -0.33 V vs. SCE. In region II of the voltammogram, stretching from ca. -0.35 to +0.2 V vs. SCE, a condensed but weakly adsorbed (physisorbed) adlayer of thymine is formed. The properties of the physisorbed phase are largely determined by lateral interactions between adsorbed molecules, whereas the substrate-adsorbate interaction has a relatively minor importance. The condensed thymine film is stabilized mainly by hydrogen bonding. This phase

has been imaged recently by in-situ STM [57]. Such high-resolution STM images point to an ordered adlayer with a unit cell which is incommensurate with the underlying Au(111) surface. The images indicate that thymine molecules are flat lying in this phase, which has a rather low coverage of ca.  $1.7 \times 10^{-10}$  mol·cm<sup>-2</sup> or about 0.074 monolayers [57].

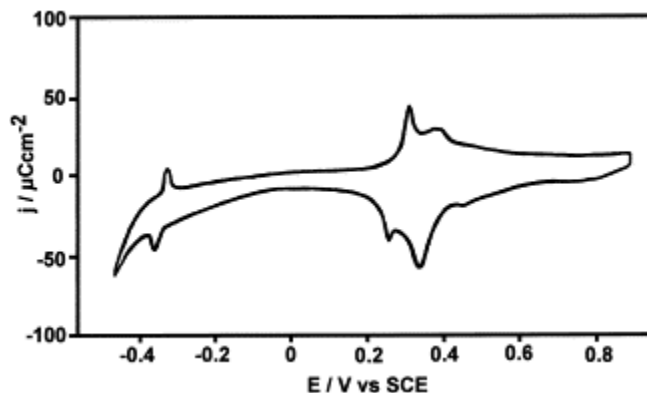


**Figure 4.2:** Cyclic voltammogram of thymine adsorption on Au(111); 12 mM thymine + 50 mM NaClO<sub>4</sub> + 10 mM HClO<sub>4</sub>; sweep rate 0.2 V/s, adopted from ref. [66].

In the potential region between +0.2 and +0.5 V vs. SCE (region III), a pronounced current peak is observed in the voltammogram, which can be related to the formation of a chemisorbed phase. The thymine coverage increases to about 0.22 monolayers in this region [57]. The potential at which the chemisorbed film is formed is linearly dependent on the pH of the electrolyte. This indicates that the formation of the chemisorbed film is connected with a deprotonation of the adsorbed thymine molecule. In agreement with this, a relatively large charge flow of ca. 40 C·cm<sup>-2</sup> is observed in region III. The potential region, in which the chemisorbed film is stable (region IV), stretches from +0.5 to at least +0.9 V vs. SCE. This chemisorbed phase has also been imaged with in-situ STM [57]. These images have been interpreted as stacks of adsorbed thymine molecules with the molecular plane perpendicular to the surface [57].

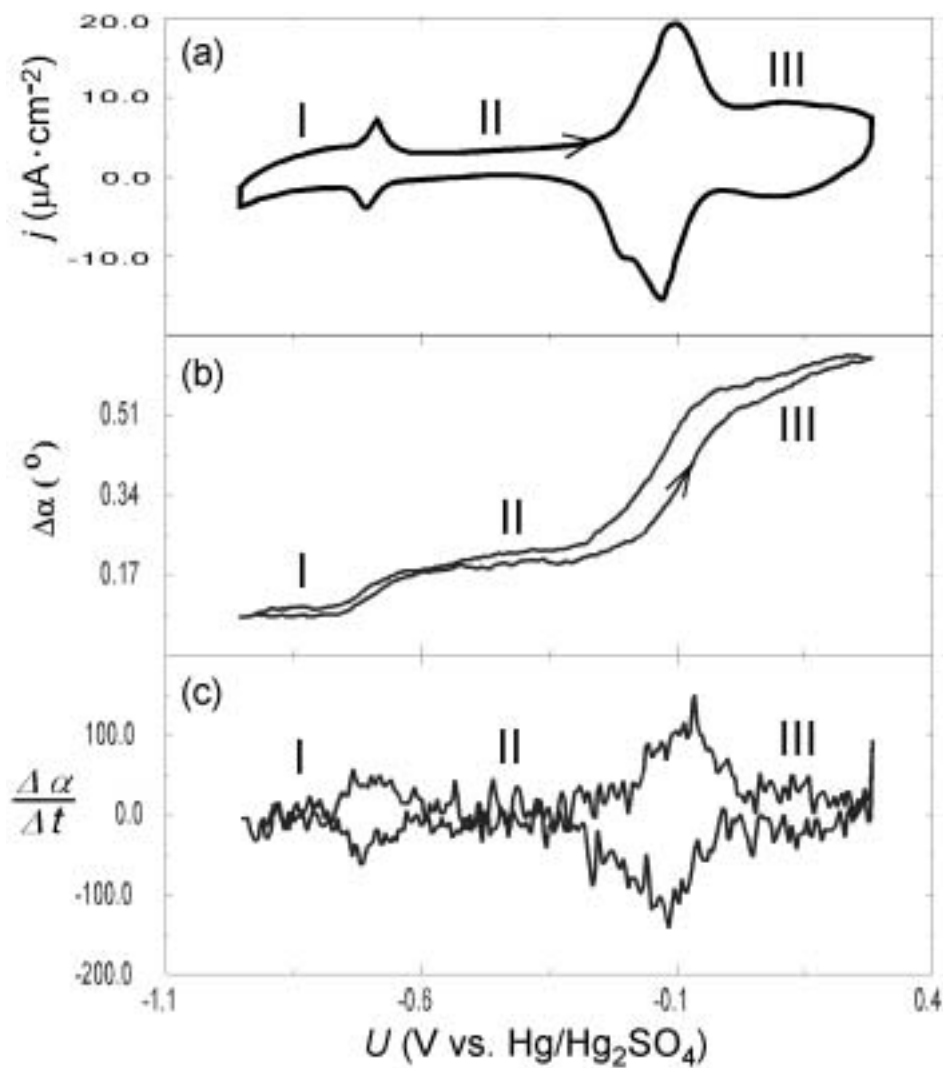


**Figure 4.3:** (a) Cyclic voltammogram of 19 mM thymine, 0.1 M NaClO<sub>4</sub>, disk Au(111) film electrode (diameter, 6 mm), scan rate 50 mV/s. (b) SPRA curve. (c) The time derivatives of the SPRA curve ( $\Delta\alpha/\Delta t$ ) vs. potential.

In Fig. 4.3a a cyclic voltammogram obtained on the Au(111) film electrode is reproduced. Clearly, the four potential regions described above are also present. The most remarkable difference between the single crystal- and the film electrodes is that the PT peaks are less sharp on the film electrode. This is to be traced back to the less perfect film electrode surface. Obviously, the adsorption of thymine occurs over a larger potential interval due to a larger amount of defects

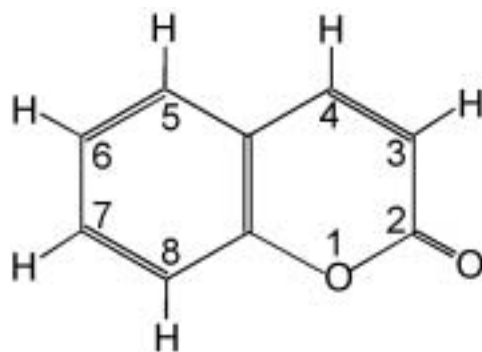
such as steps, kink sites etc. Since the CV of the Au film electrode in HClO<sub>4</sub> exhibited the characteristic features of the Au(111) surface (see chapter 3.9), this indicates that the PT of thymine is very sensitive with respect to surface defects.

Fig. 4.3b shows the in-situ SPRA measurement corresponding to the CV described above. Obviously, the curve exhibits three levels, indicating that the dielectric constant in front of the electrode undergoes two significant changes. The first change (around -0.75 to -0.65 V), corresponds to the current peaks between the regions I and II. As we explained above, the transition from region I to region II is characterized by a disorder–order phase transition between a gas-like and a condensed phase. Obviously, the formation of the condensed phase changes the dielectric constant in front of the working electrode leading to a shift of the SP resonance angle of about 0.15°. A much larger change in the resonance angle occurs in parallel with the chemisorption peak (region III, ca. -0.25 to +0.15 V).

Fig. 4.3c shows the time derivative of the SPRA curve ( $\Delta\alpha/\Delta t$ ) of Fig. 4.3b vs. the potential. Though somewhat more noisy, it closely resembles the current–potential curve of Fig. 4.3a (with the exception that the splitting of the CV due to the charging of the electrode is absent). This supports the interpretation that changes of the SP resonance indeed stem from changes of the camphor phases rather than from changes of the electrode potential or ionic contributions of the double layer.

## 4.2.2 Coumarin

Coumarin is the parent organic compound of a class of naturally occurring phytochemicals found in many plant species. This oxygen heterocycle (Fig. 4.4) is best known for its fragrance, described as a vanilla-like odor or the aroma of freshly mowed hay.

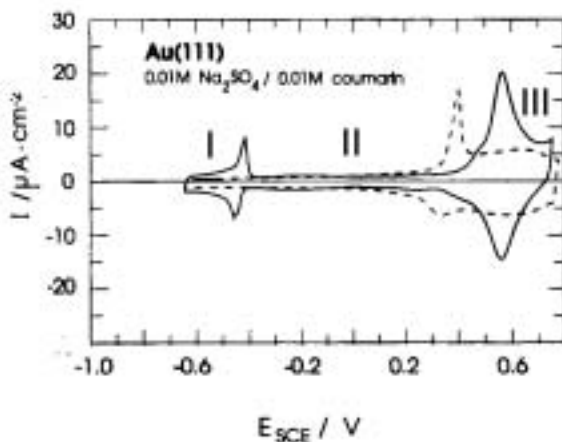


**Figure 4.4:** Coumarin molecule.

The adsorption of coumarin on Hg and Au electrodes has been studied extensively [67-70]. Like thymine, coumarin adsorption exhibits three distinct states, whereby each transition between two of these states is accompanied by a phase transition (see Fig. 4.5). But differently from thymine, the three states of coumarin are believed to be associated with three different orientations of the coumarin molecules on the surface. In the most negative potential region I, the interfacial excess of coumarin is reported to be  $6.1 \mu\text{mol}/\text{m}^2$  [68], the molecular plane of coumarin is normal to the surface, presumably oriented primarily by its dipole moment, perhaps with its carbon C(4) and C(5), or C(5) and C(6). In the most positive region III, coumarin adsorption reaches a value of about  $3.1 \mu\text{mol}/\text{m}^2$  [68]. This adsorption state has been interpreted as corresponding to a planar orientation, i.e., with the plane of the coumarin molecule parallel to that of the interface, or to an inclined one. The phase existing between these two states is believed to be a compact film, in which the coumarin carbons C(6) and C(7) point towards the surface with the whole molecular plane normal to the surface [67, 68].

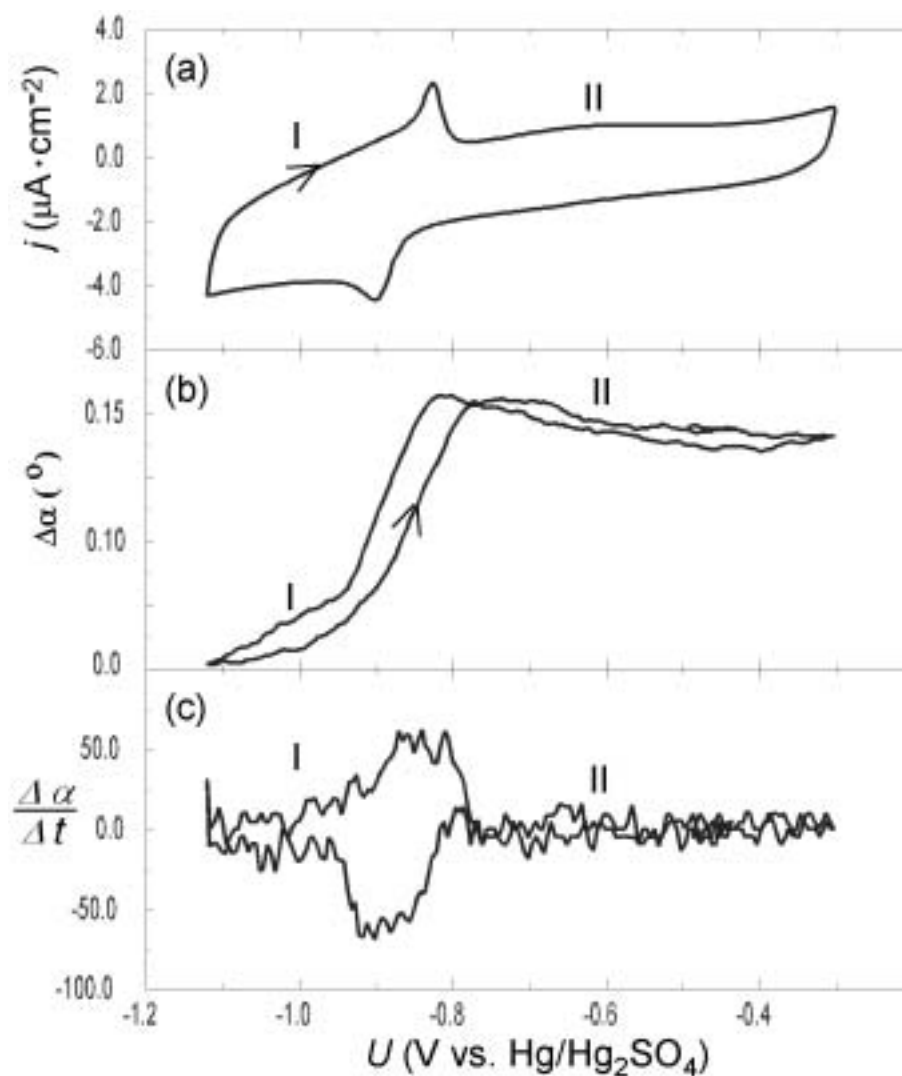
As emphasized by Hoelzle and Kolb [69], the phase transition in the positive potential region is accompanied by the lifting of the reconstruction of the Au(111) surface. Since the surface structure change might lead to difficulties in the understanding of the pattern formation process in our further studies, we only focussed on the phase transition in the negative potential region in the following

cyclic voltammetric experiments, i.e., without going to too positive potential values, and the reconstruction is not lifted.



**Figure 4.5:** Cyclic current–potential curves at scan rates of 50 mV/s (a) for Au(111) in 0.01 M  $\text{Na}_2\text{SO}_4$  before (---) and after (—) addition of 0.01 M coumarin, adopted from ref. [69].

Fig. 4.6a shows a cyclic voltammogram of the adsorption of coumarin on our Au(111) film electrode. Though region I and II are clearly discernible (-1.13 to -0.83 V vs. SMSE), the CV is less perfect than in the case of the single crystal. First, the adsorption peaks are considerably smaller, the current density in the maximum of the peak being less than twice of the double layer charging current within region II. Second, the baseline of the CV is not parallel to the voltage axis but slightly inclined in the negative end towards more negative currents. This indicates that the electrolyte is not completely free of oxygen, because coumarin solution is more viscid than the corresponding thymine or camphor (see below) containing electrolytes.



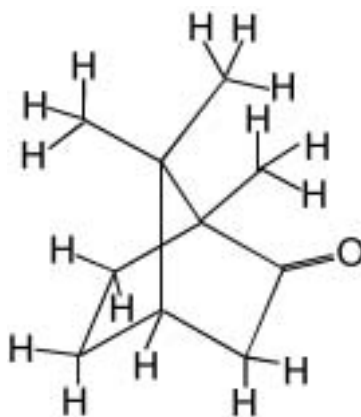
**Figure 4.6:** (a) Cyclic voltammogram of 8 mM coumarin, 3 mM NaClO<sub>4</sub>, rectangle Au(111) film electrode (30×8 mm), scan rate 50 mV/s. (b) SPRA curve. (c) The time derivatives of the SPRA curve ( $\Delta\alpha/\Delta t$ ) vs. potential.

Fig. 4.6b shows the change of the SPR angle with potential. Obviously, the transition from region I to region II is accompanied by a considerable change of the SP resonance condition. This change is larger than in the case of the negative PT in the thymine system, which is advantageous for the contrast of SP images. However, in region I, a (kinetic) hysteresis can be seen, and the SP angle is not

invariant with respect to potential variations within this region. Both features might complicate an interpretation of the SP images.

### 4.2.3 Camphor

Camphor is a molecule with the chemical composition  $C_{10}H_{16}O$ . Its structure is shown in Fig. 4.7. In pure form it crystallizes to a white solid at room temperature and possesses an aromatic pungent odor. It melts at 176 °C and boils at 209.2 °C.



**Figure 4.7:** Camphor molecule.

Camphor is known to form a two-dimensional condensed layer on Hg electrodes as well as on solid metal electrodes [71]. The formation of a two-dimensional layer at mercury electrodes was first reported by Sathyanarayana et al. [72-74]. Detailed studies of the kinetics of camphor film formation was conducted by Retter et al. [75-80]. Camphor adsorption on single crystalline electrodes was first described for bismuth by Paltusova et al. who observed pronounced adsorption peaks on smooth Au(111) surfaces [81, 82].

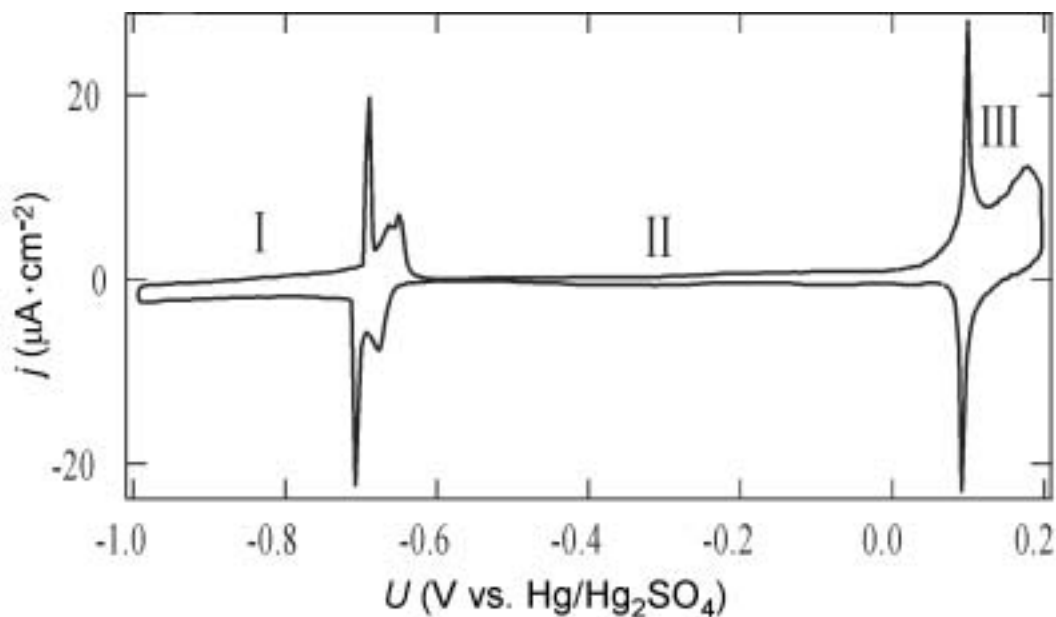


**Figure 4.8:** Cyclic voltammogram of an Au(111) electrode in a camphor/NaClO<sub>4</sub> electrolyte (5 mM camphor, 50 mM NaClO<sub>4</sub>, stationary electrode, scan rate 50 mV/s).

Striegler and Kolb demonstrated the ability of camphor to form a physisorbed two-dimensional film on Au(111) in a large potential interval [61, 83]. A cyclic voltammogram of the system 5 mM camphor, 100 mM NaClO<sub>4</sub>/Au(111) is depicted in Fig. 4.8. There are two sharp current peak pairs, which again indicate a first-order phase transition. The peak pairs encompass the potential region (region II), in which camphor forms a condensed, physisorbed film on the electrode surface. In region I the camphor coverage is negligible, while in region III a chemisorbed camphor phase exists. Upon a closer examination it is striking that the sharp current peaks at the transition between regions I and II is accompanied by a satellite peak pair at slightly more positive potentials. As discussed in references [61, 83, 84], the splitting of the negative peaks is caused by the lifting of the reconstruction of the Au(111) surface, which occurs in parallel with the positive PT. It can be prevented, when the potential is always restricted to potentials negative to region III [33, 36]. Then the Au(111) surface remains reconstructed, and a single phase transition peak marks the formation and dissolution of the condensed camphor film. For the same reasons outlined

already for the coumarin system, we here restrict our measurements to potential regions, where the Au(111) phase remains reconstructed.

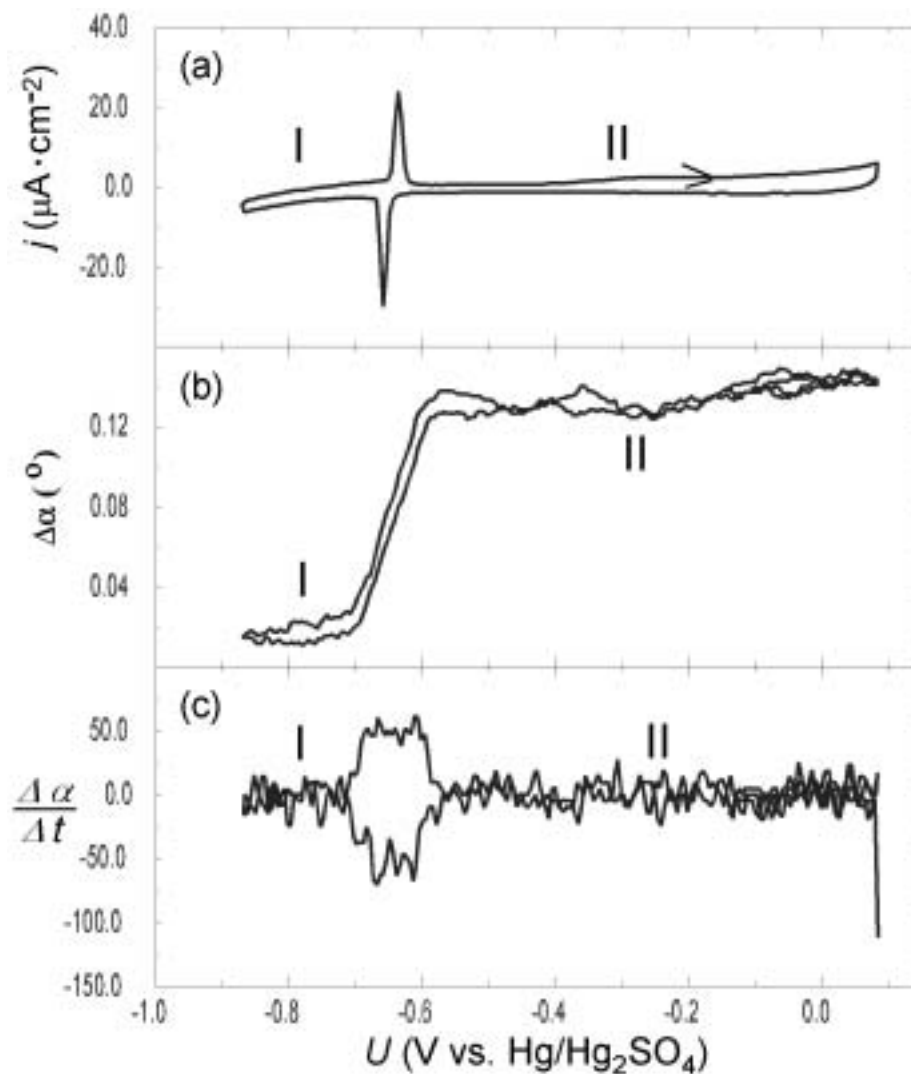


**Figure 4.9:** (a) Cyclic voltammogram of 5 mM camphor, 0.05 M NaClO<sub>4</sub>, disk Au(111) film electrode (diameter, 6 mm), scan rate 50 mV/s. (b) SPRA curve. (c) The time derivatives of the SPRA curve ( $\Delta\alpha/\Delta t$ ) vs. potential.

Fig. 4.9a shows a cyclic voltammogram of the adsorption of camphor on the Au(111) film electrode. Similar to thymine and coumarin, camphor gives rise to pronounced current peaks in the negative potential region. Moreover, at least

under our experimental conditions, these current peaks are much sharper than in the other two systems we described above. The needle-like sharp current peaks strongly indicate that also on the Au film electrode the first-order phase transition from the gas-like to the condensed phase occurs. Obviously, the condensation of adsorbed camphor molecules into an ordered film is less sensitive to structural defects of the gold surface than coumarin or thymine molecules are.

Fig. 4.9b shows the SPRA curve corresponding to the CV in Fig. 4.9a. From a comparison of Fig. 4.9a and Fig. 4.9b, it is evident that concomitant to the phase transition the SP resonance angle is changed markedly, whereas it is nearly invariant with respect to potential variations within one phase. These optical properties are ideal for our objective to distinguish the phases with SPR imaging in studies of pattern formation in systems with an S-shaped current-potential curve.

In summary, we studied the adsorption behavior of three organic compounds on Au film electrodes, thymine, coumarin and campher. All three species are known to exhibit PTs on Au(111) electrodes. In all three cases the adsorption of the molecules clearly takes place in similar potential regions on the film and on the bulk Au(111) electrode. However, in the case of campher, the formation of the condensed phase on the film electrode was accompanied by a current peak pair that was as sharp as on the (111) surface of the single crystal, whereas it was less pronounced in the other two cases. This indicates that the condensed campher phase is still formed through a first-order PT and over wide areas of the film. In contrast, the wider peaks found with coumarin and thymine suggest that here surface defects, such as steps between terraces, impede the condensation of the film over larger regions; at the defects the adsorption takes place at slightly different potentials, which causes the broadening of the peaks. Whether a first-order phase transition still occurs on the less extended (111) terraces of the film electrode cannot be unambiguously judged from the studies conducted during this thesis. For our planned studies on Turing patterns a second requirement on the organic adsorbate was that it gives rise to sufficient contrast in SPR imaging. As shown above, the campher system fulfills also this requirement. Thus it suits

our purpose, i.e., the camphor system is, in the above defined sense, a good system and was selected for the further search of a good reaction which, together with camphor, gives rise to an S-shaped current-potential curve.

### **4.3 Search for a good reaction**

Above we discussed that the second step of our strategy to design an electrochemical system which exhibits an S-shaped current-potential curve is to couple the adsorption of an organic compound, which undergoes a first-order PT upon variations of the electrode potential, to a charge transfer reaction that is inhibited differently by the two adsorbate phases. As shown in the previous section, a suitable candidate for the organic adsorbate is camphor. In this section we demonstrate how the condensed camphor layer interacts with various redox systems and select an electroactive species which exhibits the desired behavior.

The desired behavior, and thus the definition of a good reaction for our purpose is that 1) the reaction is inhibited by the condensed film formed by the camphor adsorbate on the Au(111) film electrode and that 2) the reaction possesses an appreciable reaction rate around the potential, at which the phase transition of the condensed camphor layer to the gas-like phase occurs. Note that since the condensed phase exists at more positive potentials, only reduction reactions give rise to an S-shaped current-potential curve by the above discussed mechanism. An oxidation reaction would yield a Z-shaped polarization curve, which gives rise to different and less exciting patterns than the S-shaped polarization curve.

The studies were carried out in close collaboration with Dr. Julia Oslonovitch, who performed measurements on the inhibition of different reduction reactions by a camphor adlayer on rotating Au(111) single crystal electrodes. Some of her single crystal experiments are reproduced here. For the experimental setup used with the single crystals see ref. [85].

### 4.3.1 Hexaminruthenium

Outer sphere charge transfer reduction reactions possess the simplest charge transfer mechanism: An electron tunnels from the electrode to the complexed or hydrated cation. Any adsorption step or chemical modification of the complexed ion is not involved. For this reason, we first selected a reduction reaction, which is well known to proceed via such a simple electron tunneling step, namely the reduction of  $[\text{Ru}(\text{NH}_3)_6]^{3+}$ . Current-potential curves of hexaminruthenium reduction on rotated Au(111) single crystal electrodes in the presence and absence of camphor are reproduced in Fig. 4.10.

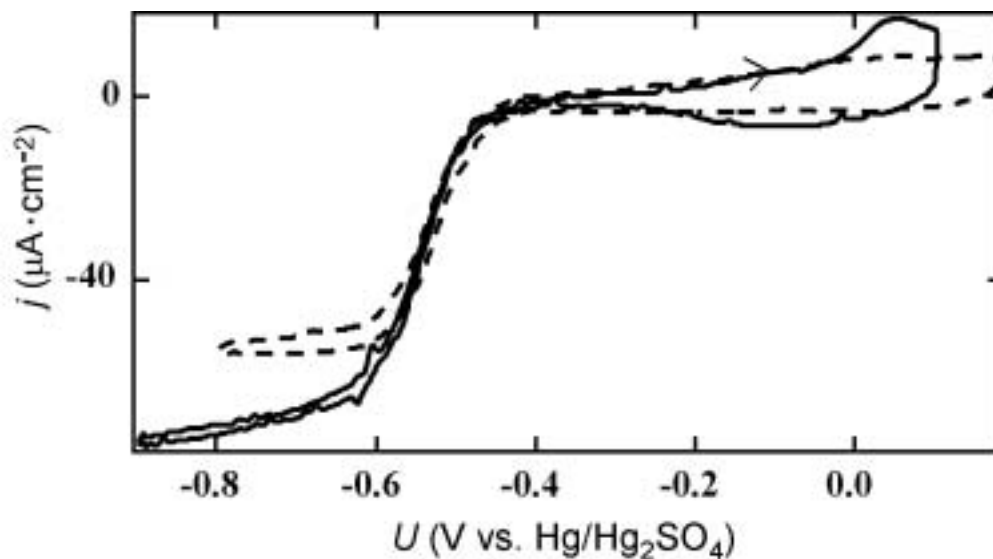


**Figure 4.10:** Cyclic voltammogram of hexaminruthenium reduction on a Au(111) single crystal in the absence (dashed line) and presence (solid line) of camphor. Electrolyte:  $7.7 \times 10^{-5}$  M  $\text{Ru}(\text{NH}_3)_6\text{Cl}_3$ , 0.1 M  $\text{NaClO}_4$ , 0, resp. 5 mM camphor, scan rate 50 mV/s, rotation speed 33 rps. (The capacitive current in the anodic region is due to the specific adsorption of chloride ions.)

Obviously, the reduction current starts to increase at approximately the same potential on the camphor covered (solid line) and on the bare Au(111) electrode (dashed line), although the onset of the current lies within the potential region in

which camphor forms the condensed phase. (The small discrepancy between both curves is to be attributed to slightly different meniscus heights and thus different mass transport conditions.) An obvious difference between the two curves is that in the presence of camphor a current peak pair is superimposed on top of the reaction current around approximately -0.6 V. This is the potential at which the phase transition of the camphor adlayer occurs, and the presence of the peak pair suggests that the condensed layer indeed still forms. There are two possible explanations of the missing inhibition of the reaction by the camphor adlayer: A) The thickness of the camphor adlayer is not sufficient to act as an effective barrier for the tunnel process. B) The reduction of hexaminruthenium is one of the fastest known electrochemical reactions. Thus, a reduction of the rate constant up to several orders of magnitude cause only a minor change of the *visible* onset of the reaction under the chosen mass transport conditions and with the chosen technique. For a more extensive discussion of this point see ref. [85]. Here, we do not discuss more quantitative aspects of the inhibition since the presented behavior clearly shows that the  $[\text{Ru}(\text{NH}_3)_6]^{3+}$ ,camphor/Au(111) system will not give rise to an S-shaped current-potential curve.

### **4.3.2 Hexacyanoferrate reduction**

Another classical electrochemical reaction with an apparently simple charge transfer mechanism is the reduction of hexacyanoferrate. Since its rate constant is about 1.5 orders of magnitude smaller than the one of hexaminruthenium reduction [85], it seemed to be a worthwhile candidate for our objective. Moreover, there are also indications in literature that hexacyanoferrate reduction is inhibited by adsorbed camphor molecules [63] as well as by other small organic molecules [64]. In addition, this redox reaction serves as a standard redox system to characterize the quality of self-assembled organic molecules (SAMs) on Au electrodes [76, 86]. The prerequisite made in all these studies is that the reaction is completely inhibited by a perfect SAM.

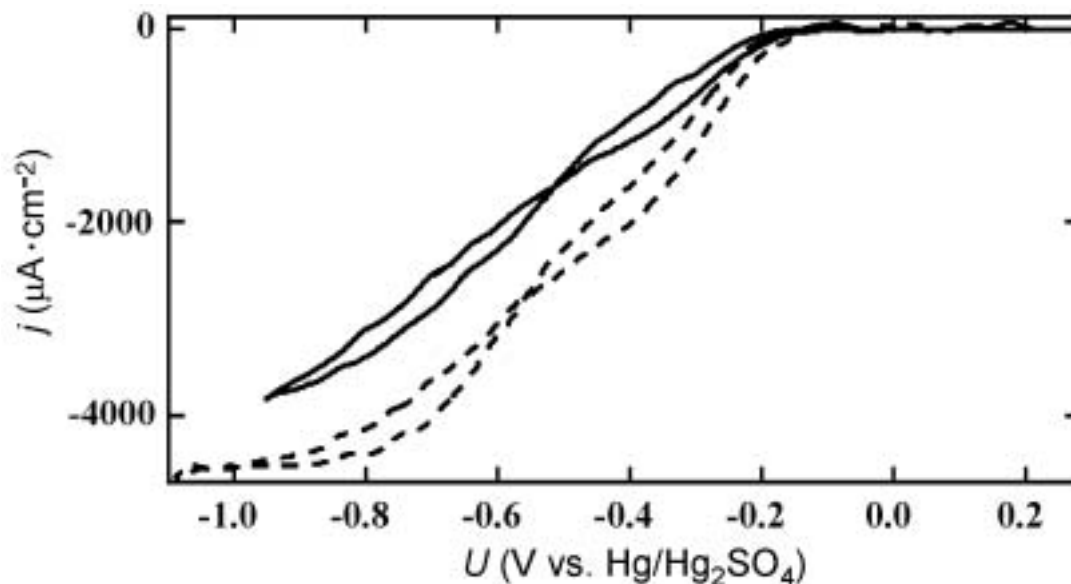


**Figure 4.11:** Cyclic voltammogram of  $K_3[Fe(CN)_6]$  reduction on a rotating Au(111) single crystal electrode in the absence (dashed line) and presence (solid line) of camphor ( $K_3Fe(CN)_6$ , 10 mM;  $NaClO_4$ , 10 mM; camphor, 5 mM; rotation rate, 27 rps).

Fig. 4.11 displays CVs of hexacyanoferrate reduction on the rotating Au(111) electrode in the absence and presence of camphor. Evidently, again, the current density is hardly changed in the potential region, in which we expect the condensed camphor film to exist. However, in contrast to the case of hexaminruthenium, no camphor PT peaks are discernible. This indicates that the film formation is affected by hexacyanoferrate reduction. Because the  $Fe(CN)_6^{3-/4-}$  redox reaction plays an important role as a standard redox system for the characterization and calibration of electrodes and is believed to proceed via a simple charge transfer mechanism, which is not in line with this observation, the camphor- $Fe(CN)_6^{3-/4-}$  system was studied – independently of questions regarding pattern formation – in detail. These studies are discussed in chapter 7. In our present context we just conclude that it does not yield the desired S-shaped current-potential curve.

### 4.3.3 Persulfate and hydrogenperoxide

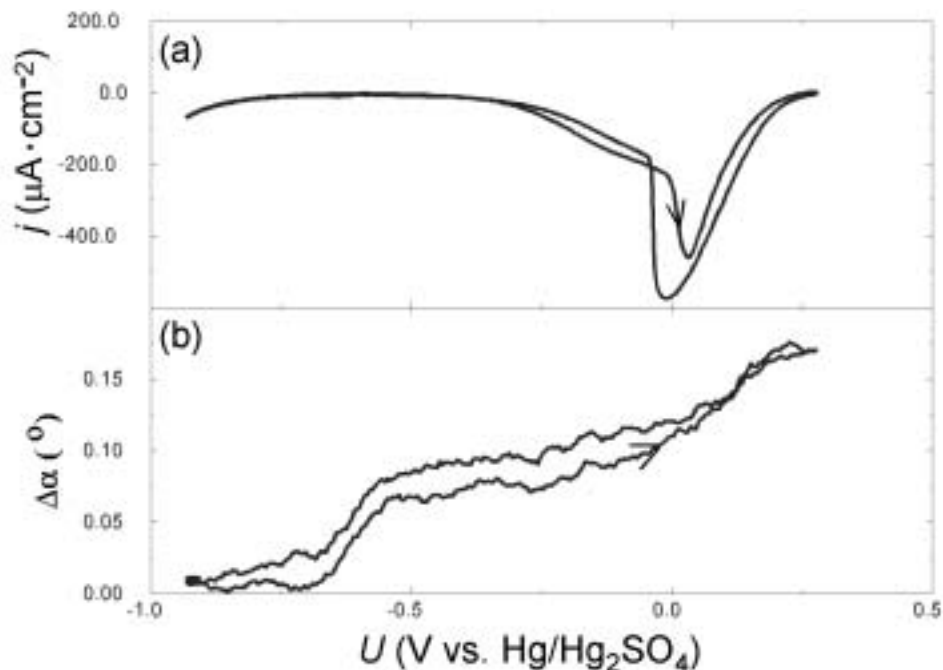


**Figure 4.12:** Cyclic voltammogram (a) and SPR shift vs. potential (b) of  $K_2S_2O_8$  reduction on a Au(111) film electrode (disk shaped, diameter 6 mm) in the presence of camphor ( $K_2S_2O_8$ , 6 mM; camphor, 5 mM;  $NaClO_4$ , 100 mM; scan rate 50 mV/s).

Another reduction reaction, which was reported to be considerably slowed down by the presence of a condensed two-dimensional camphor film, is persulfate reduction on Hg [63]. A cyclic voltammogram of persulfate reduction in the presence of camphor on a Au(111) film electrode is shown in Fig. 4.12a and the concomitantly obtained change in the SPR angle vs. potential in Fig. 4.12b. Starting at the positive turning point and scanning to more negative potentials, the current density increases considerably up to a potential at which a steep drop of the reaction current is observed, which is – upon further decreasing the electrode potential – followed by a weaker decrease. At the potential, at which we expect the PT of the camphor adlayer to occur, the reaction rate is vanishingly

small and increases only slightly for still more negative potentials. That the PT indeed still takes place can only be seen in the SPRA curve, where we recognize a step-like increase around -600 mV, as it was found in pure camphor solution (cf. Fig. 4.7). The reverse potential scan towards more positive potentials shows a similar behavior of the current density, though with a slight hysteresis compared to the negative potential scan.

One plausible reason for the sharp decrease in current density in the positive potential range of the CV would be that the camphor film forms and slows down the reduction of persulfate considerably. However, also in the absence of camphor, persulfate reduction exhibits a decrease in current density upon increasing overpotential, i.e., the current-potential curve possesses a region of negative differential resistance. This well-known phenomenon is due to double layer effects, i.e., the electrostatic interaction of the electrode surface with the negatively charged reactants around the point of zero charge. Hence, to evaluate the effect of camphor on the reaction rate in this potential region requires much more refined studies. However, for our objective, namely to tailor a system with an S-shaped current-potential curve, the potential region, in which camphor is expected to undergo a phase transition from the gas-like to the condensed film, i.e., around -600 mV, is important. Clearly, in this potential interval the current density remains very low throughout, which also has to be traced back to the electrostatic interaction between the electrode surface and persulfate ions. Thus, the persulfate and camphor combination is not a suitable system for our purpose. For this reason also the interesting question of the impact of the camphor adlayer on the reaction rate in the positive potential region, and in particular on the potential shift of the point of zero charge, which decisively influences the position of the current maximum, was not further studied in the framework of this thesis.

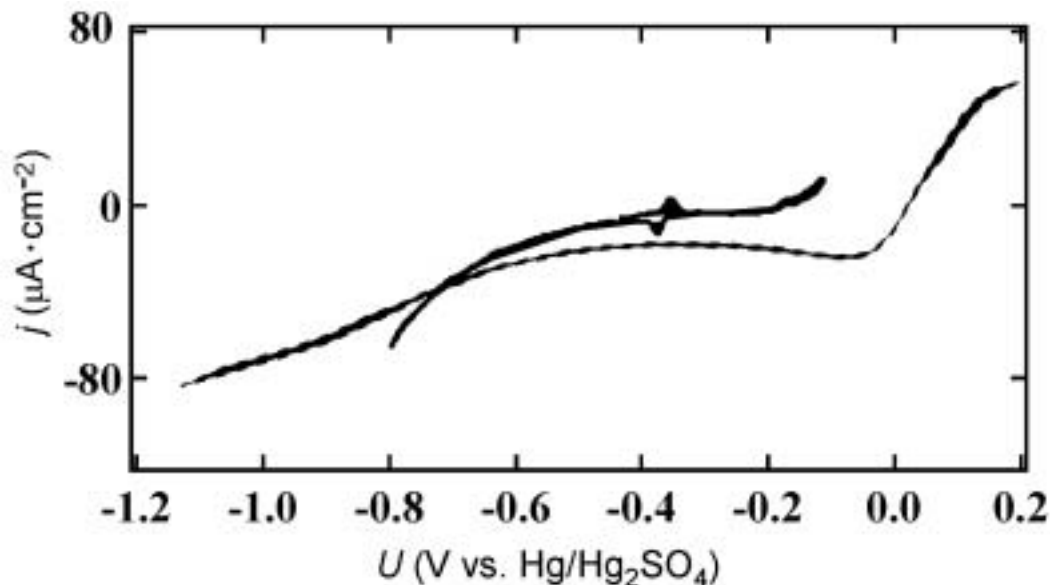


**Figure 4.13:** Cyclic voltammogram of the  $\text{H}_2\text{O}_2$  redox reaction on a Au(111) single crystal electrode in the absence (dashed line) and in the presence of camphor (solid line). ( $\text{H}_2\text{O}_2$ , 0.4 mM;  $\text{NaClO}_4$ , 0.1 M; camphor, 5 mM; scan rate, 50 mV/s; rotation rate, 28 rps).

The complications in the persulfate system arose due to double layer effects. The reduction of  $\text{H}_2\text{O}_2$  is similar to the reduction of persulfate in so far as also an O–O bond has to be broken in the course of the reaction. However, since it is a neutral species, double layer effects are absent. Thus,  $\text{H}_2\text{O}_2$  reduction seemed to be a promising candidate for our purpose.

That things were again more complicated can be seen in the CVs depicted in Fig. 4.13. They were obtained during  $\text{H}_2\text{O}_2$  reduction on a Au(111) single crystal in the absence (dashed line) and presence (solid line) of camphor. In the CV in the presence of camphor, the PT peaks are clearly visible. Compared to the pure camphor system, they are shifted by about 200 mV towards more positive potentials. This indicates that there is a strong interaction between the Au electrode and an intermediate of  $\text{H}_2\text{O}_2$  reduction – the most likely candidate seems to be OH – which apparently replaces camphor from the surface. From a comparison between the CVs in the absence and presence of camphor it becomes obvious that the current density in the presence of camphor is smaller in nearly the whole potential interval than in the absence of camphor. This is even the case

at potentials negative to the PT, at which we expected the current density to take on the values of the bare electrode. Since in the present example this is not the case, the interaction between camphor and hydrogenperoxide at the Au/electrolyte interface is more complicated than desired. Instead of more detailed investigations with this system to obtain a better understanding of the CVs, we searched for a different electroactive species which would fulfill the above defined requirements.

#### **4.4.4 Periodate**

As already mentioned, also periodate reduction on Hg was reported to be inhibited by a condensed camphor adlayer [65], which inspired us also to investigate the influence of camphor adlayers on Au on the reaction rate of  $\text{IO}_4^-$ . Fig. 4.14a and Fig. 4.14b display the CV and the SPRA vs. potential curve of the Au/camphor,  $\text{IO}_4^-$  system. In the CV it is striking that on the positive scan there is a potential interval, in which the current density is close to zero, which is flanked at both sides by sharp rises in the current density (region II). On the positive scan the behavior is similar, except that the decrease in current density is more gradual and the residual current density is somewhat larger. Most exciting in our context is the hysteresis seen in the CV at the negative end of this low current region. Connecting the two ends of this region, the resulting curve in fact traces out the shape of an S. Moreover, the potential region, in which the 'S' is observed, coincides with the potential region, in which the negative PT in the pure camphor system occurs.

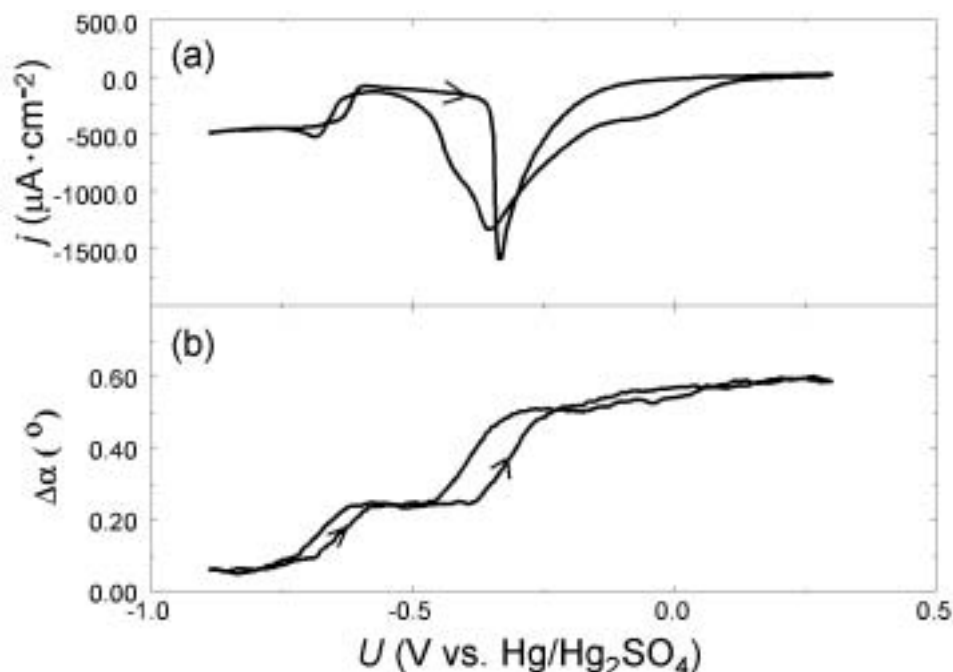


Fig.4.14: Cyclic voltammogram (a) and the SPR curve (b) of periodate reduction on a Au(111) film electrode (disk shaped, diameter 6 mm) in the presence of camphor: 5 mM camphor, 100 mM NaClO<sub>4</sub>, 5 mM NaIO<sub>4</sub>, scan rate 50 mV/s.

The SPR angle potential curve (Fig. 4.14b) exhibits, in parallel to the increase (decrease) of the current, an increase (decrease) of the resonance angle, whose magnitude is comparable to the magnitude in the pure camphor/Au system around the PT. This suggests that IO<sub>4</sub><sup>-</sup> reduction is indeed inhibited by the camphor film. A comparison of the CVs of IO<sub>4</sub><sup>-</sup> reduction in the presence (Fig. 4.14a) and in the absence (Fig. 4.15a) of camphor reveals that in the just discussed potential region the current is considerably larger in the absence of camphor. Furthermore, the respective SPR angle potential curve (Fig. 4.15b) does not exhibit the hysteresis in the potential region around 600 mV. This supports our interpretation that a) IO<sub>4</sub><sup>-</sup> reduction on Au is inhibited by camphor, and that b) around the negative PT of camphor the current-potential characteristic possesses a bistability stemming from an S-shaped polarization curve. Hence, we will use this system for our further search for Turing structures in electrochemical systems.

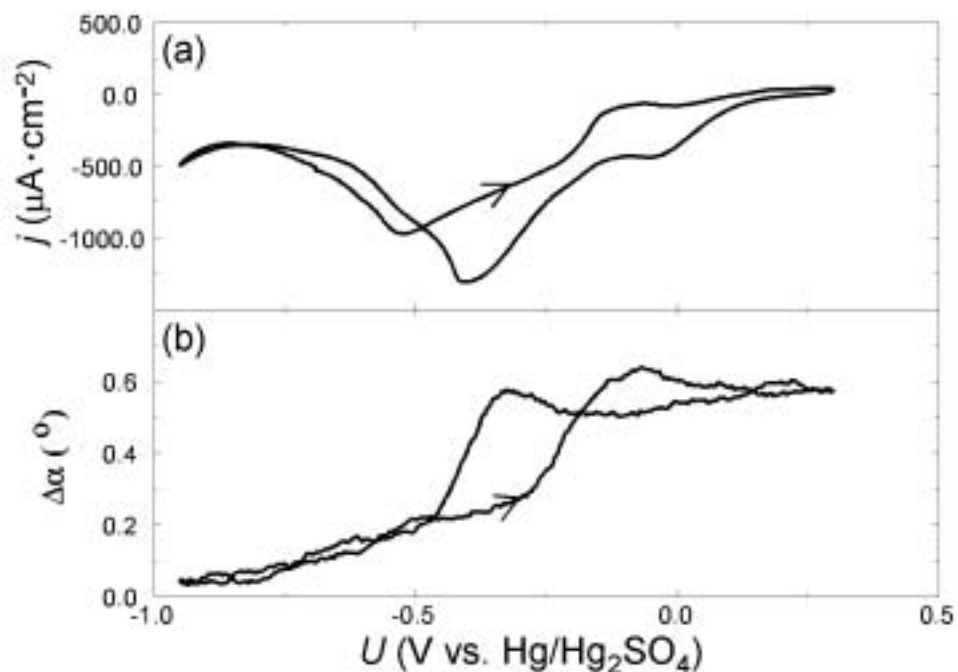


Fig.4.15: Cyclic voltammogram (a) and the SPRA curve (b) of periodate reduction on a Au(111) film electrode( disk shaped, diameter 6 mm). Electrolyte: 100 mM NaClO<sub>4</sub>, 5 mM NaIO<sub>4</sub>, scan rate 50 mV/s.

Before we turn to this aspect in the next section, it is however worthwhile to look at Figs. 4.14 and 4.15 in somewhat more detail. First, the SPRA potential curve of the camphor free system exhibits two levels in the coarsest approximation. The transition between these levels are connected with a pronounced hysteresis. The drastic change in the resonance angle must stem from a considerable change of the interfacial dielectric constant. The only interpretation in accordance with this observation is that periodate adsorbs at the electrode in the positive potential region, the two levels in the SPRA curve being thus related with the IO<sub>4</sub><sup>-</sup> covered and the bare Au surface.

Looking again at the SPRA curve of the camphor covered system, the interpretation of the three levels that can be seen there becomes clear. As already discussed, at the most negative potentials (region III), the Au electrode is free of any adsorbate. The transition to the second level stems from the condensation of

the camphor. The condensed camphor film exists in region II. It is replaced by adsorbed periodate, when the SPRA curve exhibits the second step around -0.3 V. Thus, in region I the electrode is  $\text{IO}_4^-$  covered (region I). Note that in region II the current density is much smaller than in the adjacent regions I and III, evidencing that the condensed camphor layer inhibits periodate reduction.

## Summary

In this chapter we described all the systems we have tested with respect to their ability to give rise to an S-shaped current-potential curve as the result of the interaction between the PT of an organic adsorbate and an electrochemical reaction. The Au/camphor,  $\text{IO}_4^-$  system indeed exhibited an S-shaped current-potential curve and was thus selected for the further studies on Turing patterns in electrochemical systems.